Eur. Phys. J. Plus (2011) **126**: 107
DOI 10.1140/epjp/i2011-11107-8

THE EUROPEAN PHYSICAL JOURNAL PLUS

Regular Article

FIGARO: The new horizontal neutron reflectometer at the ILL

R.A. Campbell[a], H.P. Wacklin, I. Sutton, R. Cubitt, and G. Fragneto

Institut Laue-Langevin - BP 156, 38.042 Grenoble Cedex 9, France

Received: 25 May 2011 / Revised: 6 August 2011
Published online: 11 November 2011 –

Abstract. Fluid Interfaces Grazing Angles ReflectOmeter (FIGARO) is the new horizontal neutron reflectometer at the Institut Laue-Langevin, Grenoble, France. It is a versatile, high-flux time-of-flight instrument with features suitable for a range of studies in soft condensed matter, chemistry, physics and biology both at free air/liquid interfaces and buried liquid/liquid and solid/liquid interfaces. Most of the experiments exploit isotopic contrast variation to determine the structure and composition of surface layers. Multiple chopper discs allow variable wavelength resolution, with the loose-resolution options increasing the available neutron flux for fast kinetic studies of thin films and improving the data acquisition efficiency from complex samples requiring multiple contrast measurements. It is possible to approach the interface with neutrons from below or above the horizon. The instrument is equipped with a range of sample environments including free liquid adsorption troughs, a Langmuir trough, an overflowing cylinder and a range of solid/liquid sample cells. FIGARO was launched as a user instrument in April 2009 and its success has been steadily increasing since. This article includes an introduction to the scientific case, detailed sections on the instrument components and performance, and descriptions of standard sample environments developed to date as well as some selected early scientific highlights.

1 Introduction

Figaro is a Spanish character of a French comedy that has inspired an Austrian genius to adapt the music for an Italian opera. The mix of nationalities associated with this name seemed appropriate for a new instrument at an international neutron research centre like the Institut Laue-Langevin (ILL), Grenoble, France [1]. Fluid Interfaces Grazing Angles ReflectOmeter (FIGARO) is the ILL's new high-flux, versatile, time-of-flight horizontal neutron reflectometer. The instrument was designed to deliver a complementary range of features to the neighbouring reflectometer D17, which is optimised for vertical surfaces [2]. Indeed a primary aim for FIGARO was to have the ability to perform routine experiments on adsorbed and spread layers at free liquid surfaces, which had previously not been possible at the ILL.

It has been thirty years since Hayter and co-workers proposed that neutron reflectometry (NR) could be applied to a free standing air/liquid interface [3], and the prospect was realised by Penfold and co-workers on the CRISP beamline at ISIS (UK) just a few years later [4]. To this day, NR remains the only technique that can measure directly the composition of thin films at liquid surfaces independently of their structure. Specular NR probes structure along the surface normal direction, and is specific to information contained within a few hundred nanometers from the reflecting interface. Its most distinct value in the study of soft and biological materials lies in hydrogen-deuterium substitution, which may be used either to enhance the sensitivity to a particular component at the interface or to resolve the ambiguities resulting from the loss of phase information that is characteristic of all scattering experiments. The deuterium-labelling approach allows the detailed study of multi-component systems, in which individual components cannot be resolved by X-ray reflectometry (XRR) and in addition, isotopic contrast variation often gives NR an effective structural resolution that is competitive with the superior resolution resulting from the extended q range accessible with XRR. Since the first application of grazing-incidence small-angle neutron scattering (GI-SANS) to map the in plane structure at a liquid interface [5], there remains great scope for such developments on existing reflectometers, small-angle neutron scattering machines or indeed dedicated GI-SANS instruments.

The power of NR to elucidate interfacial structures has, in the last two decades, significantly widened the range of its applications and continues to reveal new phenomena in a period of strong general expansion in the study of soft nanoscopic materials of increasing complexity. Collections of papers describing the power of the technique for

[a] e-mail: campbell@ill.eu

thin-film studies can be found, for example, in two topical Langmuir issues in 2003 [6] and 2009 [7]. However, there is considerable progress still to be made in our understanding of the physicochemical properties of interfaces, and, with the development of more powerful instruments, NR is able to probe smaller samples at shorter timescales.

For soft-matter studies, instruments with high flux able to determine structures in the nanometer range are best suited and remarkable results have been obtained, for example, on instruments like NG1 and AND/R [8] at NIST (USA), D17 [2] at the ILL and SURF [9] at ISIS. A number of instruments are being upgraded or under development both at existing and new sources, and the number of neutron reflectometers around the world is steadily increasing. For example, ISIS has recently developed on its second target station a suite of three new reflectometers: INTER, POLREF and OFFSPEC [10]. PLATYPUS at ANSTO (Australia) has also recently been commissioned [11]. The review by Teixeira *et al.*, even though focused on biology, gives an overview of the characteristics of current neutron reflectometers and projects [12]. The primary aim of the FIGARO project was to extend the range of accessible experiments at the ILL and to improve the measurement sensitivity and flexible resolution to match the needs of the user community in the following areas.

i) *Complex systems at free liquid interfaces* to study equilibrium and kinetically trapped systems at free liquid interfaces with Å resolution in the realms of soft matter (*i.e.* surfactants, polymers, colloids, etc.) and biology (*i.e.* lipids, proteins, DNA, etc.). A range of advanced sample environments is available for this purpose and continued focus is placed on developing automated and precise control of samples close to ambient conditions.
ii) *Kinetics on the time scale of seconds* to exploit the cold neutron flux and broad wavelength range of the stable reactor source at the ILL giving access to a wide dynamic bandwidth in q with very short data acquisition times, which is particularly important for structure determination and contrast matched experiments. The instrument excels at quantitative analysis of interfacial excess at low q thanks to the low natural collimation angle of the instrument combined with the ability to use cold neutrons with wavelengths up to 30 Å.
iii) *Buried liquid interfaces* to approach the interface from above or below the horizon, the latter of which can be beneficial when performing experiments at liquid-liquid interfaces. Flexibility in the instrument configuration allows a range of *in situ* equipment to be operated on top of a free liquid sample, such as rheometers, microscopes and spectrometers, to obtain complementary information.
iv) *Lateral-order and surface-induced structures* to provide valuable information on the lateral correlations of thin films, interfacial structure of liquid crystals, surface ordering of nanoparticles by off-specular scattering, and to follow kinetic processes of film growth or phase transitions. The instrument has the potential to incorporate the appropriate collimation system to deliver complementary GI-SANS measurements albeit in a limited range of lengthscales due to its short sample-to-detector distance.

Structural resolution to the Å level is achieved by measuring specular neutron reflectivity in a wide q range combined with the isotopic H/D contrast variation method. The maximum measurable q depends on the minimum reflectivity that can be measured, *i.e.*, requires maximum flux with a minimum background from the instrument and sample. However, depending on experiment, the ability to place the peak of the incident wavelength spectrum into a specific q range can also greatly decrease the measurement times required to achieve a good signal-to-background ratio, and a variable incident beam angle is highly advantageous.

Since thin (< 100 Å) films exhibit few or relatively widely spaced reflectivity oscillations within the q range measurable by NR, a large factor in flux can be gained with a relaxed resolution (up to $\mathrm{d}q/q = 15\%$) without significant loss of structural information. However, for samples with thicker interfacial layers the oscillations are more closely spaced and can benefit from higher-resolution data acquisition (down to $\mathrm{d}q/q = 1\%$). The area of the sample that can be illuminated often limits the angular resolution of the beam, but relaxing the wavelength resolution gives an additional increase in flux regardless of the sample size. To fulfill the requirements above the instrument was designed to have:

- vertical reflection plane,
- maximum available q_z range,
- minimum background (measurable reflectivities of $\sim 10^{-7}$),
- ability to measure a wide range of q_z simultaneously,
- maximum possible flux over a range of slit settings,
- reflection from above and below the sample horizon,
- simultaneous detection of specular and off-specular reflection,
- detector which can move both vertically and along the beam axis,
- flexible wavelength resolution ($1\% \leq \mathrm{d}\lambda/\lambda \leq 10\%$) for constant $\mathrm{d}\lambda/\lambda$.

2 Instrument components

FIGARO is supplied neutrons along a 28 m guide (H171), which is curved horizontally (radius of curvature $R_\mathrm{h} = 2700$ m) and downwards vertically (radius of curvature $R_\mathrm{v} = 2200$ m). The horizontal curvature results from a geometric

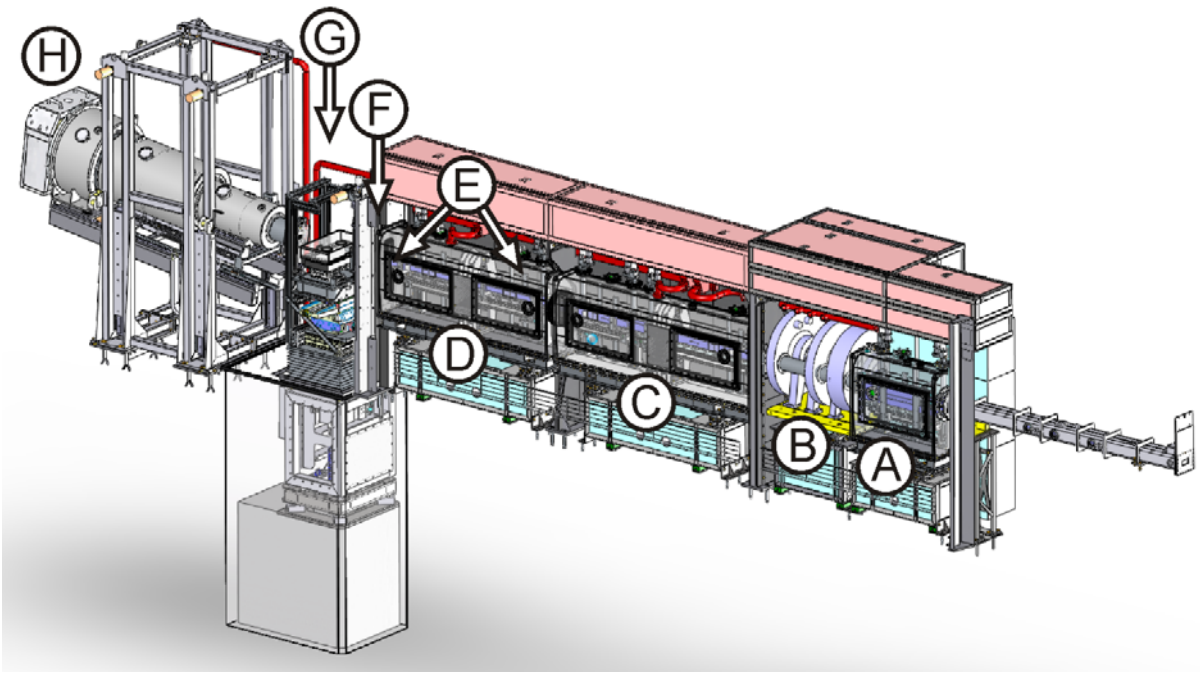

Fig. 1. Schematic of the instrument highlighting the following primary components: (A) frame overlap mirrors, (B) chopper assembly, (C) deflector mirrors, (D) collimation guide, (E) collimation slits, (F) beam attenuator, (G) sample position and (H) area detector. These components are described further in sect. 2.

practicality, which allows the neutrons to leave the reactor by an existing beam aperture. The vertical curvature is required to eliminate the direct line of sight to the reactor, which reduces the transmission of gamma rays and fast neutrons to the instrument. The sides of the guide are coated with Ni/Ti supermirrors of $m = 2$, which increases flux at all wavelengths and results in zero transmission for neutrons of $\lambda < 1.5$ Å. The top and bottom faces are initially coated with Ni/Ti supermirrors of $m = 2$ but gradually fall to a nickel coating in parallel with the vertical divergence, which results in zero transmission for neutrons of $\lambda < 1.3$ Å. The dimensions of the guide at the reactor exit are 80 mm × 15 mm (w × h) and the height is increased linearly to 30 mm at the start of the instrument in order to capture the full beam divergence.

The beam arrives at the start of the instrument at a downward collimation angle of 0.67° relative to the horizontal. This choice of beam angle was determined by the practical requirements of building the instrument and the necessity to deliver a range of collimation angles for the reflection up and down configurations while having limited deflection angles possible due to the supermirror coatings of the deflector mirrors. Note that the natural downwards collimation angle of the instrument itself has since been defined as 0.62° relative to the horizontal, which is different by 0.05° to the orientation of the beam delivered to the start of the instrument in order to avoid pointing the collimation slits back to a hole in the vertical beam profile due to the presence of a beam shutter (see sect. 3.2).

Figure 1 shows a schematic of FIGARO and its principal components, including two frame overlap mirrors, a 4-disc chopper assembly, beam deflector mirrors, a collimation guide, collimation slits, a beam attenuator, the sample position and detector with an evacuated flight tube. The first collimation slit (S2) is positioned between the second deflector mirror and the collimation guide, and the second collimation slit (S3) is positioned between the collimation guide and the sample position. The horizontal distances and lengths of the instrument components are listed in table 1. The instrument components before the sample position (*i.e.* those described in sects. 2.1–2.4 below) are enclosed in vacuum housings pumped down to a pressure of $< 10^{-2}$ mbar. The frame overlap mirrors, deflector mirrors, collimation guide and area detector/flight tube are each supported by two motors on vertical shafts. The angle of each component is controlled to a precision of ±0.001°.

2.1 Frame overlap mirrors

Frame overlap mirrors are required to remove neutrons above a certain wavelength so that the long and short wavelengths in sequential pulses are always separated in time. The mirror is a transmission filter: neutrons with wavelengths above a predefined value are removed from the incoming white beam by reflection from a nickel-coated silicon wafer. Neutrons with shorter wavelengths are transmitted through the mirror with minimal losses.

Table 1. Horizontal positions of the centre of various instrument components relative to the reactor guide exit and lengths. The chopper 1–sample distance is 5906 mm, the S2–S3 inter-slit distance is 2165 mm and the S3–sample distance is 368 mm.

Component	Centre (mm)	Length (mm)
Reactor guide exit	0	
Neutron feed guide	1397	2754
Frame overlap mirrors	3287	900
Chopper guide 1 (C1/C2)	3893	150
Chopper guide 2 (C2/C3)	4201	234
Chopper guide 3 (C3/C4)	4554	434
Lead diaphragm	4899	82
Deflector mirror M1	5714	1445
Deflector mirror M2	6883	800
First collimation slit (S2)	7352	6
Collimation guide	8328	1876
Lead diaphragm	9380	104
Second collimation slit (S3)	9517	6
Beam attenuator	9567	20
Sample table	9885	500
Flight tube	11426	2582
Area detector	12769	

The location of two frame overlap mirrors (SD-H, Germany) is indicated in fig. 1A and a photo is shown in fig. 2A. Each mirror sits in a 900 mm guide section of 80 mm × 30 mm (width × height), made of Borkron glass (Schott N-ZK7 specification, including $\geq 11\%$ B_2O_3) with a nickel coating ($R > 98\%$) on the top and bottom surfaces and Ni/Ti supermirror coating of $m = 2$ ($R > 94\%$) on the sides. One guide has a nickel-coated silicon wafer inclined downwards at angle of 2° relative to the incident beam to give a wavelength cut-off of 20 Å (coated length of wafer = 859 mm) and the second guide has another Si wafer inclined at 3° relative the incident beam to give a cut-off of 30 Å (coated length of wafer = 573 mm). To avoid damage from direct exposure to the high neutron flux from the feed guide the uncoated front faces of each glass assembly are protected with thin boron-based shields that absorb neutrons. The first half of the top guide face does not have a supermirror coating in order to avoid neutrons with long wavelengths reflecting first off this surface then off the downstream side of the mirror back into the beam (without this modification the device would transmit neutrons at twice the critical wavelength). The nickel-coated silicon wafers are constructed of three pieces with the largest piece spanning in the centre of the guide so that the maximum flux does not cross a step. The wafer coatings are made of natural nickel ($d = 2000$ Å, $R > 99\%$).

2.2 Chopper assembly

A time-of-flight reflectometer at a reactor source requires choppers to deliver distinct pulses of neutrons down the instrument [13,14]. The neutrons in each pulse have a range of velocities, and the detector measures their wavelength according to the time they are detected relative to the time they leave the choppers. The four-disc chopper assembly (EADS Astrium GmbH, Germany; figs. 1B and 2B) pulses the neutron beam in the wavelength range required whilst giving a choice of wavelength resolutions ($d\lambda/\lambda$) to the user. The motivation for having different separations of the controlling chopper pairs is that a constant $d\lambda/\lambda$ can be obtained using zero chopper opening from the following equation:

$$\frac{\delta t}{t} = \frac{\delta D'}{D} + \frac{\phi}{2\pi} \cdot \frac{q}{q_{\min}}, \tag{1}$$

where t is the travelling time of the neutron, D' is the chopper separation, D the time-of-flight distance, ϕ the chopper opening, $q = 4\pi \sin\theta/\lambda$ is the momentum transfer, θ is the incident angle of neutrons on the sample and λ is the neutron wavelength. That is to say, compared with a single chopper pair of fixed 10 cm separation (like on the neighbouring D17 reflectometer), a factor of up to about 8 in flux can be gained with zero chopper opening and hence constant $d\lambda/\lambda$ simply by choosing a controlling chopper pair with a wider separation. This method has the added advantage

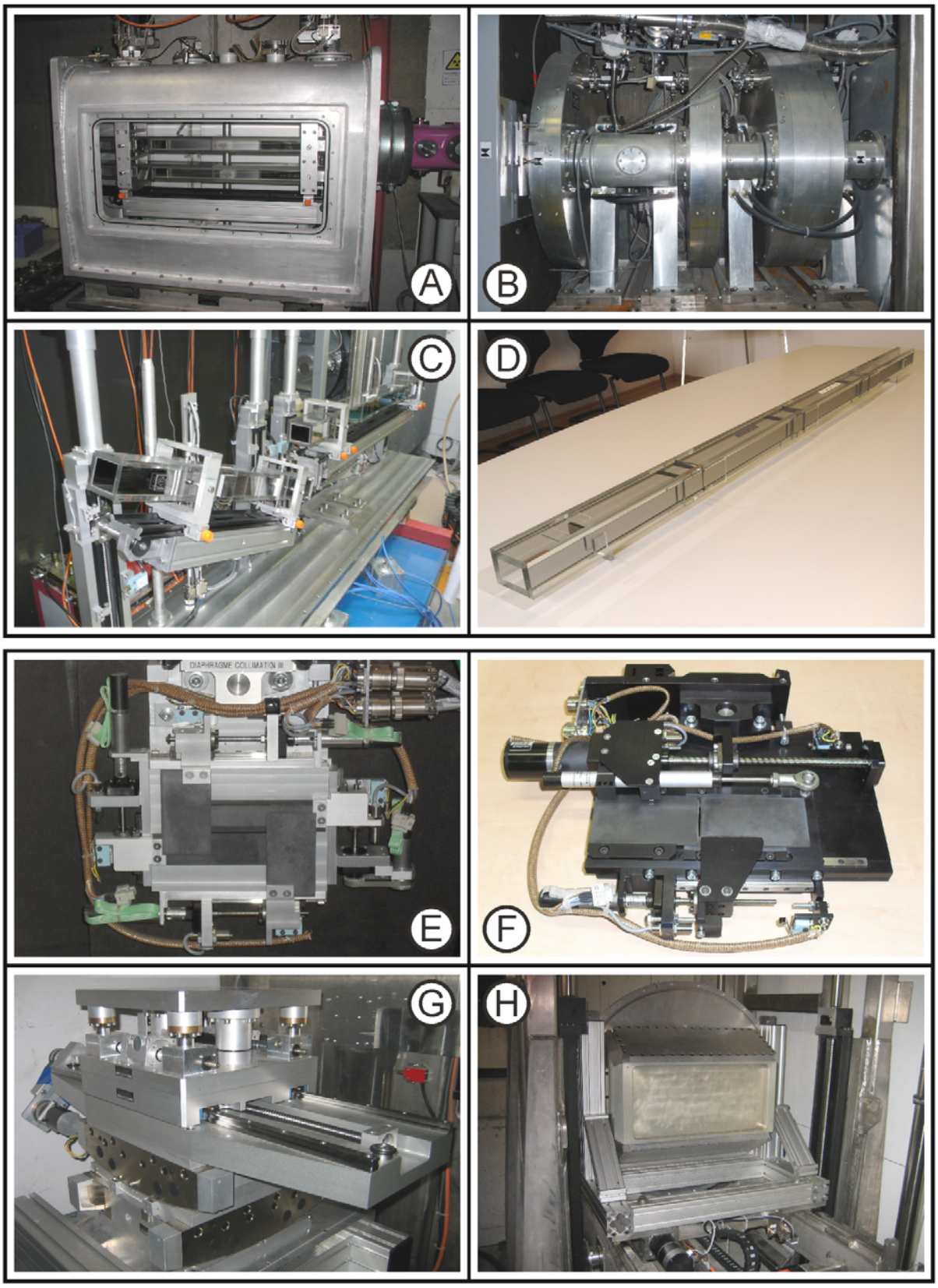

Fig. 2. Photographs of the primary components of the FIGARO instrument: (A) frame overlap mirrors inside their vacuum casing, (B) chopper assembly, (C) deflector mirrors, (D) collimation guide, (E) one of the sets of collimation slits, (F) beam attenuator, (G) sample position equipment and (H) area detector. Labels correspond to the position of the component in fig. 1.

Table 2. Distances involved with the six chopper configurations, where the first chopper-to-sample distance is 5906 mm, $D1$ is the active mid chopper-to-sample distance, $D2$ is the active mid chopper-to-detector distance, and the sample-to-detector distance is 2884 mm.

Wavelength resolution	Controlling pair	Separation (mm)	$D1$ (mm)	$D2$ (mm)
1.2%	C1/C2	97.2	5856	8740
3.0%	C2/C3	247.2	5681	8565
4.2%	C1/C3	347.2	5731	8615
5.6%	C3/C4	447.2	5331	8215
8.6%	C2/C4	697.2	5456	8340
9.8%	C1/C4	797.2	5506	8390

Table 3. Speeds and phases of the six chopper configurations for three different frame overlap mirror configurations (30 Å, 20 Å and 16 Å). The instrument is generally used in a configuration with pulses split into 1000 time channels of 40 μs (for 16 Å cut-off), 50 μs (for 20 Å cut-off) or 75 μs (for 30 Å cut-off) in addition of an electronic delay of 3750 μs per pulse.

Wavelength resolution	Frame overlap	Speed (rpm)	C2 Ph (deg)	C3 Ph (deg)	C4 Ph (deg)
1.2%	30 Å	743	45.0	30.0	39.5
3.0%	30 Å	758	−16.0	29.0	21.0
4.2%	30 Å	755	20.0	45.0	37.0
5.6%	30 Å	792	0.0	−7.5	37.5
8.6%	30 Å	779	−6.5	12.0	38.5
9.8%	30 Å	756	12.5	21.0	45.0
1.2%	20 Å	1116	45.0	29.0	38.0
3.0%	20 Å	1139	−16.0	29.0	20.5
4.2%	20 Å	1132	20.0	45.0	37.5
5.6%	20 Å	1187	1.5	−7.5	37.5
8.6%	20 Å	1169	−7.5	12.0	37.5
9.8%	20 Å	1135	12.5	21.0	45.0
1.2%	16 Å	1393	45.0	28.5	37.5
3.0%	16 Å	1421	−16.0	29.0	20.5
4.2%	16 Å	1416	20.5	45.0	38.0
5.6%	16 Å	1485	2.5	−7.0	38.0
8.6%	16 Å	1461	−8.0	11.5	37.0
9.8%	16 Å	1418	13.0	21.0	45.0

that the choppers do not need to be re-phased when changing collimation angles. The option of configuring a single chopper pair to have non-zero opening can be used in addition to increase further the flux.

The choppers discs of 800 mm diameter and 45° opening are made from fibre reinforced composite coated with ^{10}B and have a transmission of 10^{-10} above 2 Å. The chopper system is evacuated by an additional turbo pump to $< 10^{-3}$ mbar. The chopper system is configured so that all four discs spin continuously in synchronisation. Any pair of discs can be employed to define the neutron pulses while the other two are phased so that they do not to affect the pulse shape. The chopper speed varies depending on the desired wavelength range of the pulses. To date the options 2–16 Å, 2–20 Å or 2–30 Å have been used.

Table 2 contains a list of relevant distances for the six different chopper configurations used to generate neutron pulses with wavelength resolutions in the range $1.2\% \leq \mathrm{d}\lambda/\lambda \leq 9.8\%$. Table 3 lists the speed and phase data for the three different frame overlap mirror configurations commissioned to date (*i.e.* 30, 20 and 16 Å). In each case, the controlling pair has a phase difference of 45° (*i.e.* zero opening) while the other two choppers are phased so as not to impinge on the neutron pulses accordingly. This approach allows the user to maximise the neutron flux through relaxing the wavelength resolution to 9.8% for very thin films < 100 Å where there are no sharp features in the reflectivity profiles. In addition, high-resolution measurements of thick samples up to 1000 Å are possible using the 1.2% resolution configuration.

Table 4. Summary of the deflector mirror configuration and the reflecting sample surface geometry for the five collimation angles commissioned to date.

Collimation angle	Deflector mirror configuration	Sample geometry
0.62	None	Reflection up
2.0	M1 - downward deflection	Reflection up
3.8	M1 and M2 - downward deflections	Reflection up
−0.62	M1 - upward deflection	Reflection down
−2.7	M1 and M2 - upward deflections	Reflection down

2.3 Deflector mirrors

To measure a broad q range at horizontal free liquid surfaces, two supermirrors (M1 and M2 in table 1) are used to deflect the incident beam that emerges at the sample position away from the natural collimation angle of 0.62° downwards from horizontal. The additional feature for maximum flexibility in experiment design is that the mirrors can deflect the incident beam either upwards or downwards in order to approach the reflecting interface from below or above the horizon. We define the "reflection up" configuration as when the neutron beam emerges at the sample position at a downward collimation angle relative to the horizontal to be reflected upwards by the sample surface (*e.g.*, a free standing air/liquid interface) and the "reflection down" configuration as when the neutron beam emerges at the sample position at an upward collimation angle relative to the horizontal to be reflected downwards by the sample surface. Table 4 summarises the deflector mirror configuration and the reflecting sample surface geometry for the five different collimation angles commissioned to date.

Two Ni/Ti supermirrors ($R > 80\%$, Swiss Neutronics, Switzerland; figs. 1C and 2C) made of Borkron glass, 50 mm high, 1445 mm (M1) and 800 mm (M2) long (to account for divergence at the sample), have top and bottom coatings of $m = 4$ to allow the incident beam to be deflected up to 1.7° without significant loss of intensity. Thus, the maximum angles of incidence achievable are 4.0° reflection up (two mirrors deflecting downwards each with an incident angle of 0.85°) and −2.7° reflection down (the two mirrors correspondingly deflecting upwards), which is asymmetric due to the natural downward collimation angle of 0.62° to the horizontal. Higher incident angles can be achieved on solid samples by rotating the sample additionally up to ±5° using the transverse sample stage goniometer. The mirrors also collimate the incident beam width from 80 to 68.2 mm (M1) and 68 to 61.4 mm (M2).

2.4 Collimation guide

A collimation guide (Swiss Neutronics, Switzerland; figs. 1D and 2D) made of Borkron glass is 1876 mm long and focuses the beam horizontally from 59.5 to 40 mm. The vertical sides are coated by $m = 4$ ($R > 75\%$), and the top and bottom faces each carry three sintered boron carbide baffles (spaced at equal intervals of 469 mm positioned about the centre of the guide) to prevent reflections in the vertical plane. The free-guide height is therefore 40 mm and the beam exiting at the end is limited by collimation slit S3 to a maximum height of 16 mm, which is far in excess of the requirement for experiments. The collimation guide is positioned downstream of the deflector mirrors so that the collimation slits reduce the background created by off-specular scattering from the $m = 4$ coatings of the deflector mirrors.

2.5 Collimation slits

The two beam-defining collimation slits (called S2 and S3; figs. 1E and 2E) have four blades to define the left, right, top and bottom side of the neutron beam. The blades are made of 2 mm thick sintered boron carbide highly enriched with ^{10}B, which are operated either directly or via synchronous drives due to space constraints. The blades are separated in the direction of the beam by 2 mm in order to retain the option on occasions to set them to an overclosed configuration. The precision of the blade movements was measured using an optical position sensor (Keyence, Japan, LKG-152) normally used on the instrument to automate the height alignment of free liquid surfaces. It was shown that the direct and belt connections each had a precision of ±1 μm in the same direction, and that due to backlash the direct connections had a precision of ±6 μm and the belt connections had a precision of ±10 μm when changing direction. The instrument software was therefore configured to maximise precision by always approaching specified positions in a positive direction.

2.6 Beam attenuator

A fully automated oscillating beam attenuator (figs. 1F and 2F) was designed in house at the ILL and was constructed by Eria (Grenoble, France). It is used for the recording of direct beam measurements in cases where the full beam intensity would saturate the detector and distort the time-of-flight spectrum. This distortion results from a space-charge effect, which occurs when neutrons arrive in the detector at a rate that is faster than the rate of dissipation of the ionised gas molecules, whose presence decreases the local electric field and thus the efficiency of neutron detection. In a time-of-flight spectrum on FIGARO the effect is most pronounced for neutrons with wavelengths in the peak range of 5–6 Å. The device attenuates the beam by a constant factor independent of wavelength. A narrow vertical opening oscillates horizontally over the full width of the incident beam at constant speed during data acquisition to record the true time-of-flight spectrum reduced in intensity by a single attenuation factor. The beam attenuator has blades made of sintered boron carbide backed with 0.2 mm gadolinium strips whose horizontal opening can be varied to a precision of $\pm 20\,\mu$m, as necessary. The minimum opening, before reflections off the gadolinium blades significantly distort the recorded TOF spectrum, is $150\,\mu$m. Optimisation of the horizontal opening allows transmission measurements to be recorded typically in < 20 min using the maximum flux on the detector, and the intention is to automate fully the normalisation of neutron reflectivity measurements in the future. The fully open position of the attenuator (45 mm width $\times$ 25 mm height) does not impinge on the incident beam during reflectivity measurements and all the attenuator functions, including oscillation speed and travel limits, are controlled directly from the instrument software.

2.7 Sample position

The principal components of the sample position are two flexible crossed goniometers, two vertical translation stages, a horizontal translation stage, and an active anti-vibration control unit (figs. 1G and 2G). The centre of rotation of the transverse goniometer is 196 mm above the sample table, which is sufficient for the mounting of most sample environments. The main challenge in specifying the sample position components was to translate a load of up to 1000 kg while minimizing the level of transmitted vibrations to free liquid samples. There are two vertical translation stages, one coarse (500 mm travel) and one fine (32 mm travel). The reason is that the course stage re-positions the sample according to changes in collimation angle because the beam emerges from the collimation slits at different absolute heights, and the fine stage re-positions the sample independently according to changes in the sample alignment. The horizontal translation stage (500 mm travel) allows sample changers to be used, *e.g.*, currently there are the assemblies for 6 free liquid troughs and a rack of 7 solid/liquid cells. Low-frequency vibrations are damped by the steel frame of the sample table, which sits in a 2 m deep hole and is embedded in concrete. Higher-frequency vibrations above 1 Hz are damped by an active anti-vibration table (Halcyonics, Vario45), which has a maximum active load of 300 kg. This damping is necessary for free liquid samples, on which any external vibrations can significantly increase the amplitude of capillary waves thus significantly reducing reflectivity. The entire sample area is additionally enclosed by a frame of acoustic foam shielding behind which a combination of concrete and lead reduces further the ambient noise level [15,16].

2.8 Area detector

A new area detector was designed and constructed by the ILL Neutron Detector group for FIGARO with the aim of increasing the efficiency and count rate capability (figs. 1H and 2H). The 512×256 mm (width $\times$ height) area detector is constructed from a single block of aluminium, with 64 squared, 25 cm long channels cut into it. Each tube is filled with 8 bars of ^{3}He and 2 bars of CF_4, and contains a $15\,\mu$m Stablohm wire of 250 mm active length, which detects neutrons by charge division. The high voltage of 2500 V applied to each wire gives a vertical position resolution of 2 mm on the detector. Each channel has a width of 6.9 mm, with a 0.5 mm wall of aluminium between adjacent channels, which gives rise to a horizontal position resolution of 8 mm. The main advantage of this design over conventional delay line-type detectors is the increase in segmentation, that is, each wire is contained within a separate gas volume, thus limiting charge saturation to individual wires. The electronic dead time of the detector is further reduced because all 64 wires are connected to individual amplifiers. Advantages of using aluminium rather than steel as the detector material are that the front detector window (5 mm thick) has higher transmittance of neutrons, allowing for higher detection efficiency of particularly long wavelength neutrons, and the material does not activate for long periods.

The detector is attached to a 2.5 m evacuated flight tube equipped with a circular (150×0.5 mm, diameter $\times$ thickness) aluminium window at the sample end and a 32 mm thick aluminium plate at the perimeter of the detector end. The flight tube is lined with boron carbide-dosed rubber and contains three windows made of the same material to reduce further the detected background scattering. The detector and flight tube are mounted on a steel rail on a stainless steel frame using two motors which are used to control the height and angle of the detector relative to the sample. The vertical translation range of the detector is ± 300 mm and without the flight tube the sample to detector distance can be varied between 1.2 m and 2.9 m. The accessible angular range of the detector relative to the undeflected beam for a collimation angle of 0.62° downwards from horizontal is 6° at a sample-to-detector distance of 2.8 m and 15° at a distance of 1 m.

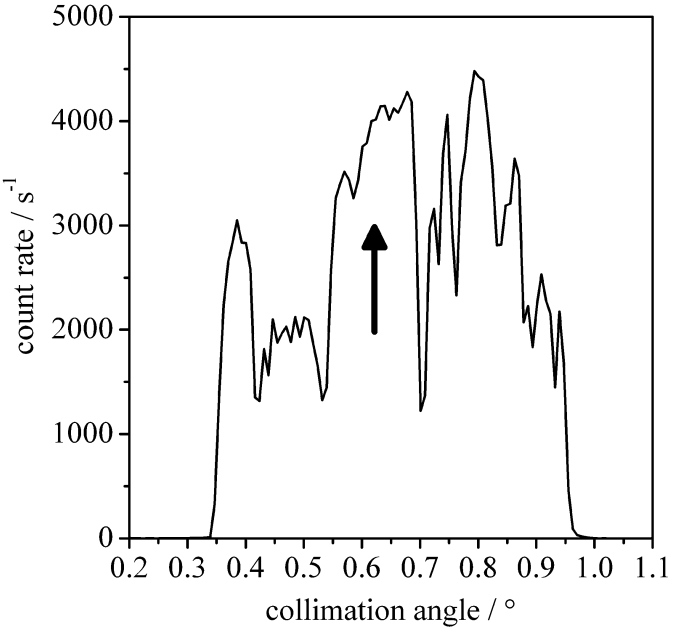

Fig. 3. Vertical beam profile showing the count rate on the detector for an angular scan of the collimation slits. The arrow indicates a broad maximum in the neutron intensity corresponding to the natural downwards collimation angle of the instrument.

3 Instrument performance

3.1 Neutron flux

The white beam flux before the instrument was recorded as $1.4 \times 10^{10}\,\mathrm{n\,cm^{-2}\,s^{-1}}$ with a gold foil measurement in October 2008. During experiments the flux is determined by the chopper pair chosen: the flux on the sample using the widest chopper pair (9.8% $\mathrm{d}\lambda/\lambda$) is about 8 times higher than when using the narrowest chopper pair (1.2% $\mathrm{d}\lambda/\lambda$). As an example, a valid configuration for a measurement using the popular 5.6% $\mathrm{d}\lambda/\lambda$ chopper pair at the collimation angle of 0.62° with S2 and S3 openings of 0.8 mm × 40 mm and 0.4 mm × 30 mm (both $h \times w$), respectively, gives a neutron count rate of $\sim 4 \times 10^4\,\mathrm{n\,cm^{-2}\,s^{-1}}$ corresponding to an illuminated area of $\sim 40\,\mathrm{cm^2}$ on the sample.

3.2 Beam profiles

A vertical profile of the neutron beam may be recorded by measuring the direct beam on the detector while carrying out an angular scan of the collimation slits. Figure 3 shows an example of a beam profile recorded with narrow collimation slits (vertical openings of 0.3 mm and widths of 40 mm) and a chopper pair corresponding to 1.2% $\mathrm{d}\lambda/\lambda$. The arrow marks the natural downwards collimation angle of the instrument of 0.62° to the horizontal, which has been defined by pointing the collimation slits back to a reflecting face of the curved neutron feed guide to the instrument as indicated by the broad maximum in the vertical beam profile. Such scans have led to a better understanding of the various guide reflections that contribute to the beam, and have allowed several collimation angles to be configured by pointing the collimation slits back to the same position on the feed guide. The pronounced hole in the profile to the right of the broad maximum (and arrow) in fig. 3 results from a gap in the neutron feed guide to the instrument due to the presence of a beam shutter, and the sharper peaks at collimation angles further from 0.62° result from reflections off the various frame overlap and chopper guides closer to the sample position.

3.3 Time-of-flight spectra

The time-of-flight (TOF) spectrum on FIGARO, resulting from the vertical cold source at the ILL, has its maximum intensity at around 5–6 Å depending on the collimation angle. Figure 4 shows TOF spectra recorded for the 5.6% $\mathrm{d}\lambda/\lambda$ chopper pair for the five collimation angles commissioned to date: 0.62° (A), 2.0° (B) and 3.8° (C) "reflection up" and −0.62° (D) and −2.7° (E) "reflection down". The same slit openings were used to highlight the relative flux of neutrons for these five configurations and, as can be seen, the total loss of flux due to the mirror deflections does

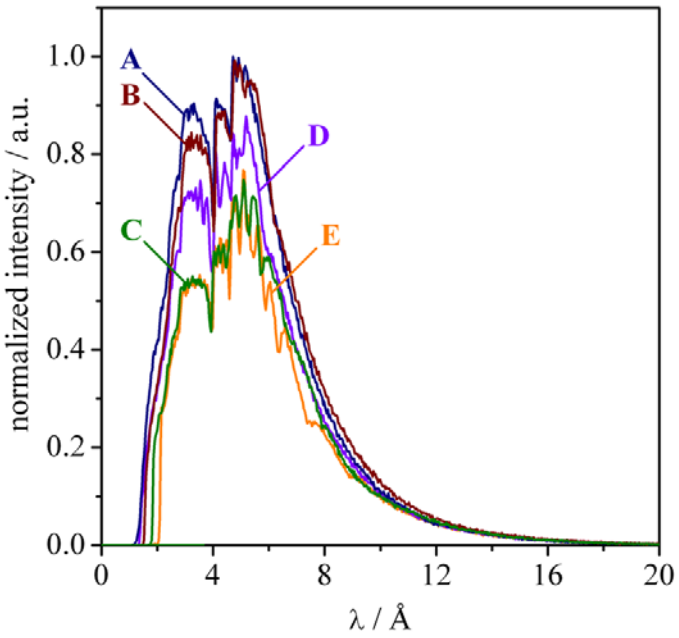

Fig. 4. TOF spectra recorded for the 5.6% $d\lambda/\lambda$ chopper pair at the natural collimation angle of 0.62° (A), a single deflection down to give a collimation angle of 2.0° (B), a double deflection down to give a collimation angle of 3.8° (C), a single defection up to give a collimation angle of −0.62° (D) and a double defection up to give a collimation angle of −2.7° (E).

not exceed 16% for one deflection or 40% for two deflections. The greatest reduction in intensity of neutrons occurs at fairly low wavelengths (< 6 Å) resulting from roughness and imperfections of the deflector mirrors which give rise to off-specular scattering (configurations B–E), and there is total loss of neutrons of very low wavelengths (< 2 Å) due to the critical wavelengths of the supermirrors at the employed deflection angles of ∼ 0.8° (particularly notable for configurations C and E). For all five collimation angles the wavelengths of the aluminium absorption lines match values previously published [17].

Figure 5 shows TOF spectra recorded at the natural downward collimation angle of 0.62° with the 30 Å (C, green) and 20 Å (B, red) frame overlap mirrors. The choppers spin 50% faster when using the 20 Å frame overlap mirror to allow the user to favour flux over q range. The instrument has been configured so that each frame overlap mirror delivers neutrons until the stated value (20 or 30 Å), the mirror cuts off the neutrons sharply by the stated value +10%, and the chopper speeds are configured such that the next neutron pulse begins at the stated value +20%. Also shown is a TOF spectrum from a 16 Å (A, blue) frame overlap mirror option where the 20 Å frame overlap mirror is tilted to provide a neutron cut-off at a lower wavelength. In this case the choppers can spin proportionately faster to favour flux further for fast kinetic measurements.

3.4 Wavelength corrections due to gravity

Calculations on the effects of gravity on the cold neutrons are incorporated into the data reduction software package COSMOS; the programs runs on the free runtime version of LAMP, which can be downloaded from the webpages of the instrument on the ILL's website [1]. The effects relate to the fact that the colder neutrons travel more slowly and therefore fall a greater distance vertically during their time-of-flight than fast neutrons. Figure 6 shows the drop of several millimeters experienced by the cold neutrons by the time they reach the detector. Note that the drop is much more pronounced than that observed on other horizontal reflectometers in use today which do not use neutrons with wavelengths as long as $\lambda = 30$ Å.

Without correction, such beam dispersion due to gravity on a reflectometer with a vertical reflection plane would produce a significant systematic error in the calculation of q which therefore needs to be taken into account. Neutrons follow a parabolic path through the two collimation slits arriving slightly before the sample centre at an angle larger than the straight-line path defined by the collimation. The position affects the illuminated surface area and the change in incident angle of neutrons on the sample means the true value of q is altered. In addition, a beam of the coldest neutrons will have travelled through the choppers lower down at a smaller angle to the horizontal. These effects result in a need for a correction to the chopper delay angle and the chopper opening. Figure 7 shows the definition of some key variables associated with the problem.

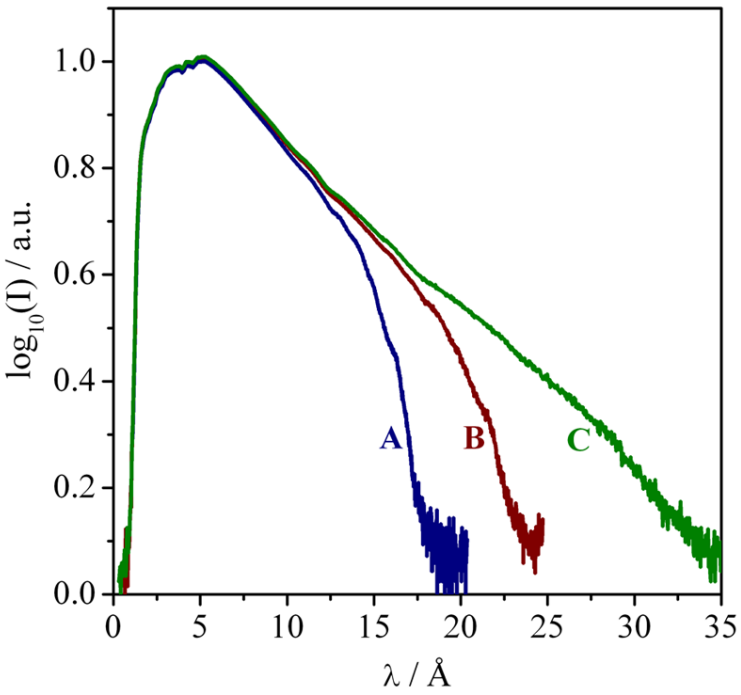

Fig. 5. Time-of-flight spectra showing different frame overlap mirror configurations: 16 Å cut-off from using the 20 Å mirror in a tilted configuration (A, blue), 20 Å mirror (B, red) and 30 Å mirror (C, green). These data correspond to orientations of a nickel-coated silicon wafer relative to the incident beam of 1.6°, 2.0° and 3.0°, respectively. Data are normalised and presented on a log scale.

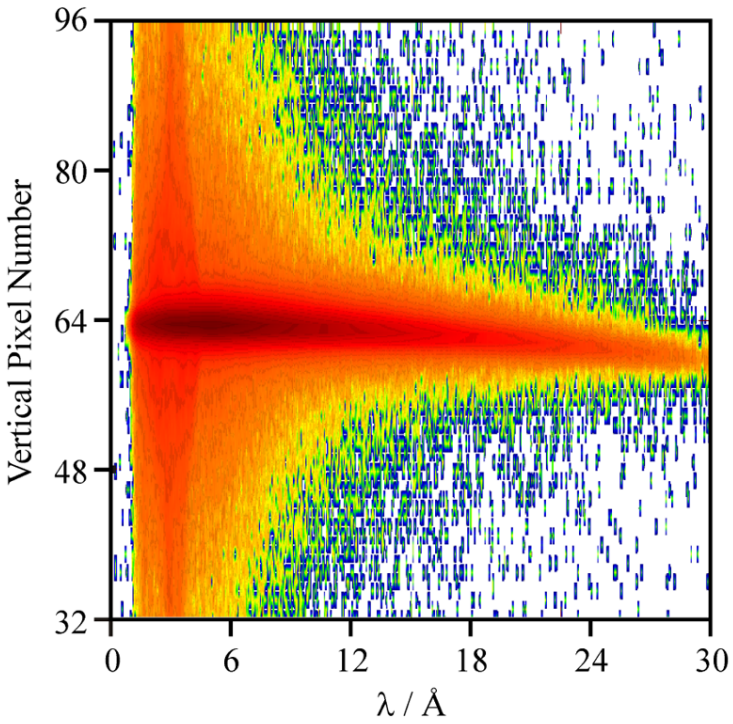

Fig. 6. Direct beam image recorded on the detector with a time-of-flight distance of 8.2 m showing a 6 mm drop of the cold neutrons at 30 Å (1.2 mm/pixel).

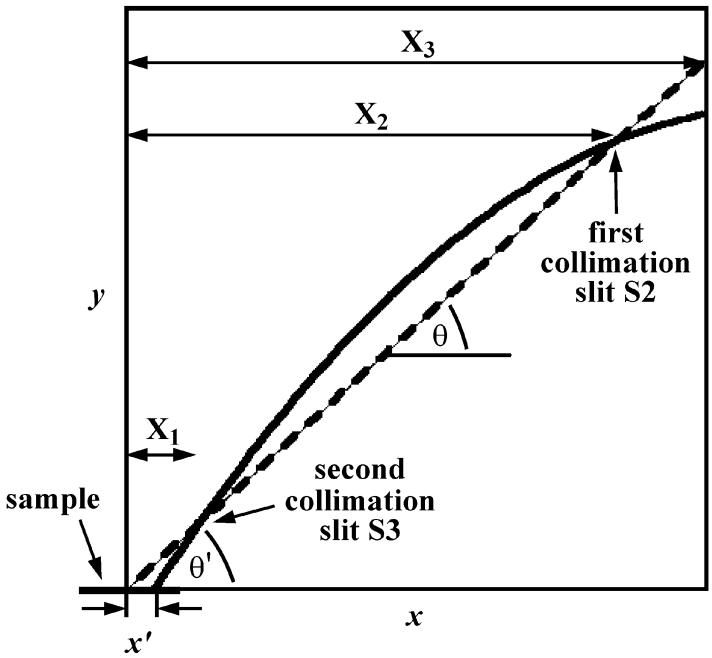

Fig. 7. The dashed line is the straight-line path through the slits centred on the sample at theta to the horizontal and the solid line shows the path of a neutron affected by gravity. The horizontal distances x, x', X_1, X_2 and X_3 are defined from the centre of the sample, and y is the vertical distance from the sample centre.

The equation of motion describing the parabolic path of a neutron is:

$$y = (x - x') \cdot \tan(\theta') - k(x - x')^2, \tag{2}$$

where y is the height above the sample, x is the horizontal distance from where a neutron at infinite velocity would strike the centre of the sample, x' is the horizontal distance from the centre of the sample to where the neutron falling under gravity strikes the sample, θ is the angle through the collimation slits of a neutron at infinite velocity, θ' is the angle of the neutron falling under gravity, $k = g/2v^2$ is the characteristic inverse length of the problem, g is the gravitational acceleration and v is the neutron velocity. The unknown quantities x' and θ' are functions of the slit positions assuming that the wavelength is defined by the horizontal velocity component alone.

$$\tan(\theta') = \frac{\tan(\theta) + \left[\dfrac{k(X_1 - x')^2}{X_1}\right]}{1 - \left(\dfrac{x'}{X_1}\right)}, \tag{3}$$

where θ is the incident angle on the sample of infinitely fast neutrons, X_1 is the S3-sample centre distance and x' is the smallest value solution to the quadratic equation

$$\left(\frac{1}{X_2} - \frac{1}{X_1}\right) \cdot kx'^2 + \left(\frac{\tan(\theta) \cdot \left(\dfrac{1}{X_1} - \dfrac{1}{X_2}\right) + X_2}{X_1 - \dfrac{X_1}{X_2}}\right) \cdot x' + (X_1 - X_2) \cdot k = 0. \tag{4}$$

Now the position and gradient of neutrons are defined anywhere along the path with respect to the wavelength. For example, putting values of the appropriate parameters in eq. (4) such as $X_1 = 368\,\text{mm}$, $X_2 = 2533\,\text{mm}$, $X_3 = 5331\,\text{mm}$ (for the 5.6% $\mathrm{d}\lambda/\lambda$ chopper pair) and $\theta = 0.62°$ (the undeflected collimation angle of the instrument), we calculate $\theta' = 0.666°$, $x' = 22.6\,\text{mm}$, chopper delay angle correction $= 0.73°$ and a vertical drop at the choppers of 3.9 mm for 30 Å neutrons. Note that the correction of the incident angle of neutrons on the sample is related to whether the instrument is used in the "reflection up" or "reflection down" configuration (the former increases and the latter decreases θ with respect to λ).

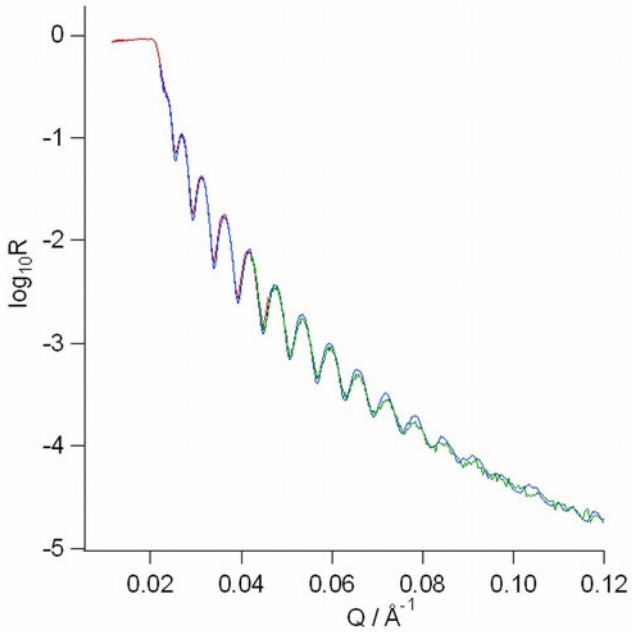

Fig. 8. Neutron reflectivity from a 100 nm nickel-coated glass sample using the 5.6% $d\lambda/\lambda$ chopper pair at incident angles of 0.62° (red), 2.0° (blue) and 3.8° (green). Figure produced using Motofit [19].

3.5 Time-of-flight calibrations

There are currently three principal time-of-flight calibrations routinely carried out on the FIGARO instrument.

A) The sample-to-detector distance, DET, is calibrated by measuring the vertical pixel position of direct and reflected beams for a horizontal sample in the range DET = 1.2–2.9 m. When the flight tube has been removed the detector, oriented vertically, can move horizontally towards the sample on its trolley. The difference in pixel positions between the direct and reflected beams is then fitted linearly and extrapolated to zero to define DET = 0 m.

B) The *opening offset* is the relative phase angle between two controlling choppers such that there is no direct line of sight for infinitely fast neutrons, *i.e.*, there is a projected opening angle of zero. To calibrate this parameter with respect to each controlling chopper pair and each collimation angle, a multilayer sample is aligned to give a Bragg reflection at a wavelength of λ_{Bragg} in the range 4–5 Å, followed by measurement of the TOF channel of the peak as a function of DET in m to calculate the wavelength:

$$\lambda_{\mathrm{Bragg}} = \sigma \times K \times \mathrm{gradient}, \tag{5}$$

where $K = \lambda v = 3.956 \times 10^{-7}\,\mathrm{m^2\,s^{-1}}$, v is the neutron velocity in $\mathrm{ms^{-1}}$, σ is the time channel width in s, and λ is in m. From the measured wavelength, the change in the projected opening angle, ω, of the controlling chopper pair during which time neutrons of wavelength λ_{Bragg} traverse the controlling chopper pair can be calculated, according to

$$\omega = \frac{\lambda_{\mathrm{Bragg}} \times cht \times 360}{K \times \tau}, \tag{6}$$

where *cht* is the chopper separation in m, and τ is the chopper period in s. Lastly, the intensity of the Bragg peak at a fixed detector distance DET is measured as a function of the chopper phase to obtain the real zero opening time for the given wavelength from the x intercept of the linear plot. The *opening offset* is the actual opening corresponding to no line of sight for infinitely fast neutrons, which can then be calculated using

$$\textit{opening offset} = x - \mathrm{intercept} + \omega. \tag{7}$$

C) *Poff* is a parameter attributed to twice the angle between the angle of the choppers at the pickup event and when the beam is open, *i.e.*, TOF = 0 s. It is possible to measure this parameter by recording a plot of the TOF channel number of the same Bragg reflection peak with respect to the chopper speed, where

$$\textit{Poff} = 720 \times \sigma \times \mathrm{gradient}. \tag{8}$$

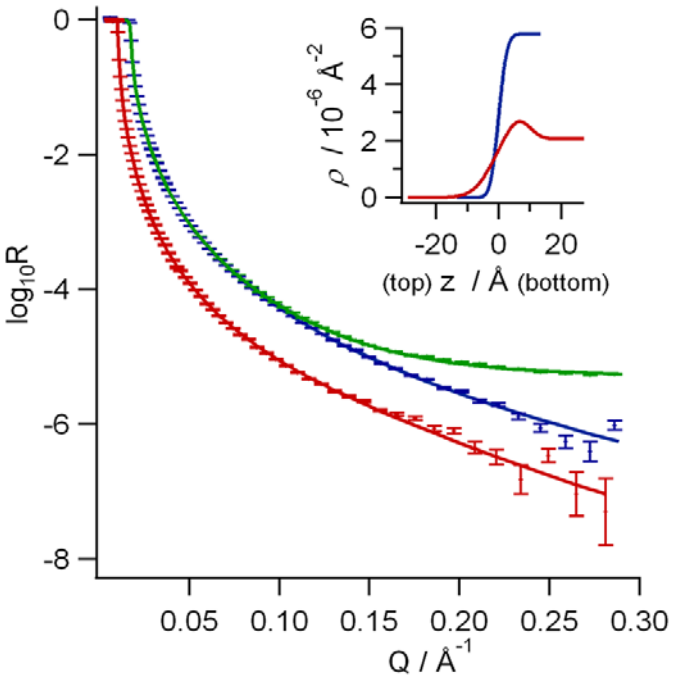

Fig. 9. Reflectivity profiles of the air/silicon interface with background subtraction (red) and the air/sapphire interface both with (blue) and without (green) background subtraction. Scattering length density profiles corresponding to the optical matrix fits (solid lines) to the data are shown in the inset. Figure produced using Motofit [19].

Alternatively a 100 nm nickel-coated glass sample is used to record reflectivity profiles with pronounced Kiessig fringes [18] for each controlling chopper pair and each collimation angle (see example in fig. 8). *Poff* has been systematically fitted to data measured of the same sample independently on the D17 reflectometer and elsewhere, which is a procedure that results in an uncertainty in q of $< 1\%$ over the whole q range accessible on the instrument. We note that small variations in the neutron trajectory through the choppers and the guide system for different controlling chopper pairs and collimation angles result in different effective opening offset and *Poff* parameters, which currently need to be characterised individually.

3.6 Detector performance

The maximum acceptable count rate of the detector is primarily limited by saturation of neutrons with wavelengths in the peak range of 5–6 Å due to a space-charge effect (see sect. 2.6). The effect is routinely controlled during direct beam measurements through the use of the beam attenuator described above, but the issue has also been experienced during measurements of films at the air/D_2O interface when using a high-flux instrument configuration. The detector performance has been characterised in a series of measurements to determine the acceptable maximum count rates for user experiments. The measurements were carried out by varying the horizontal opening of the oscillating beam attenuator at different fixed values of the collimation slits S2 and S3. This approach was taken to quantify the distortion of the TOF spectra with increasing neutron intensity as a function of the area illuminated on the detector. A limit of 3% distortion in the shape of the TOF spectrum was deemed the maximum acceptable deviation. The total acceptable count rate depends on the area illuminated on the detector and therefore the openings of the collimation slits. The maximum acceptable count rate increases with the slit opening as the beam is dispersed more over the area of the detector. As the vertical illumination of neutrons on the detector at a collimation angle of 0.62° is typically around 3–6 mm, whereas at a collimation angle of 3.8° the beam height on the detector may be around 8–16 mm, the maximum acceptable count rates currently employed in user experiments are ~ 0.5–$1 \times 10^4\,\mathrm{n\,s^{-1}}$ in the former case and ~ 2–$4 \times 10^4\,\mathrm{n\,s^{-1}}$ in the latter case.

3.7 Reflectivity spectra

Full q range reflectivity spectra of adsorbed layers or spread films of material are typically recorded in between 10 minutes and 1 hour on FIGARO depending on the scattering contrast, sample size and coverage of the interfacial material. Figure 9 shows a reflectivity profile of the air/silicon interface recorded at two incident angles (0.62° and 3.8°)

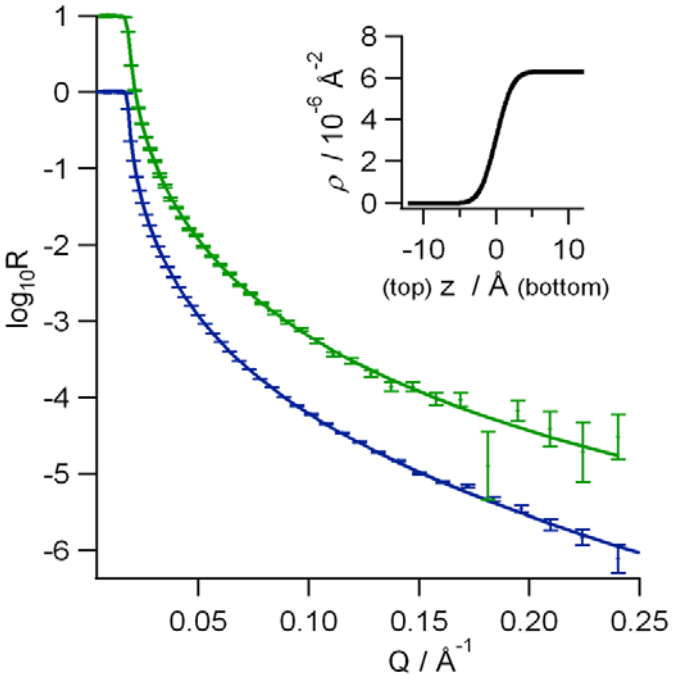

Fig. 10. Reflectivity profiles of the air/D_2O interface recorded with 5.6% $d\lambda/\lambda$ for a data acquisition time of 40 min (blue) and with 9.8% $d\lambda/\lambda$ for a data acquisition time of just 1 min (green; offset for clarity). A scattering length density profile corresponding to the optical matrix fit (solid line) to the data is shown in the inset. Figure produced using Motofit [19].

using $d\lambda/\lambda = 5.6\%$ for a total data acquisition time of 2 h (red). Here we demonstrate that measurable reflectivities of $\sim 10^{-7}$ are achievable in realistic time scales for a sample with low interfacial roughness. Also shown are reflectivitity profiles of the air/sapphire interface both with (blue) and without (green) background subtraction indicating that the inherent instrument background measured simultaneously on the area detector can be subtracted to good effect. Figure 10 (blue) shows low error bars in a reflectivity profile of the air/D_2O interface recorded at the same two incident angles using $d\lambda/\lambda = 5.6\%$ for a generous data acquisition time of 40 min.

3.8 Fast data acquisition

Figure 10 (green) shows reflectivity data of the air/D_2O interface recorded with loose resolution over a q range of 0.005–0.25 $Å^{-1}$ for a total data acquisition time of just 1 min: 10 s at an incident angle of 0.62° and 50 s at an incident angle of 3.8°. Note that additionally the instrument currently takes ~ 90 s to change between these two configurations during which time a minimum of 14 motors are used to reposition a variety of instrument components (*e.g.*, mirrors, the sample table and beam defining slits). Work is underway to minimise this downtime through improving motor efficiencies, although in many experiments a multi-position sample changer can be used to measure more than one sample at a given incident angle between changes of the instrument configuration.

The FIGARO instrument excels in particular at low-q data acquisition where measurements as short as 1 s have been recorded and fitted to good effect in user experiments through exploiting high-flux features of the instrument such as the loose resolution and reduced q range. This is achievable because high reflectivities of partially deuterated interfacial layers at the free surface of air contrast matched water can be rapidly recorded as a result of the use of cold neutrons with wavelengths of up to 30 Å and the low natural collimation angle of the instrument of 0.62°. In this case a direct relationship exists between the product of the scattering length density and thickness of a single-component adsorption layer, and data from a mixed-component layer may be co-refined with additional NR contrasts or data from X-ray reflectivity or ellipsometry to quantify the interfacial composition. Figure 11 shows the product of the scattering length density and layer thickness of two different polymer/surfactant adsorption layers at the air-water interface as a function of the total data acquisition time for a given zero time stamp. The figure is a representation of how long it is necessary to record such data to achieve a given precision. Uncertainties dominated by counting statistics are on the order of just 5–10% for total acquisition times of < 15 s, and it can be seen that in < 1 min the product can be determined to $< 2\%$ discrepancy of the value recorded at the long data acquisition time limit of a few minutes. Further examples of fast data acquisition may be found in the featured early scientific highlights in sect. 5.

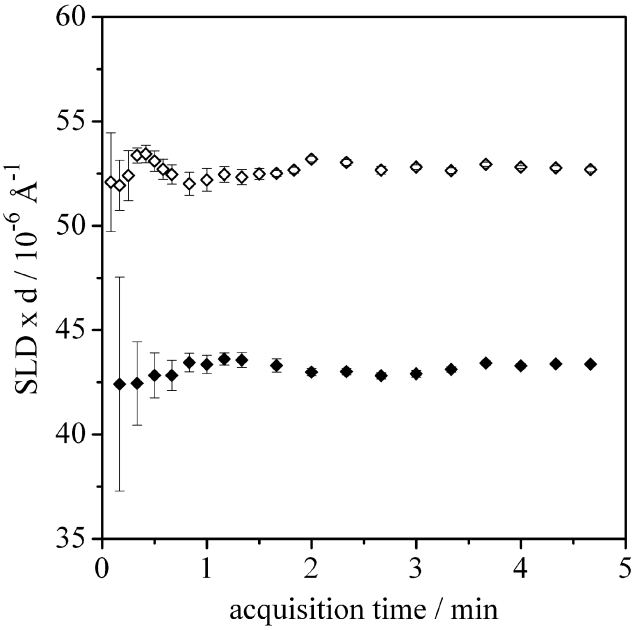

Fig. 11. Fitted NR data of two polymer/surfactant mixtures in air contrast matched water recorded on an overflowing cylinder: 400 ppm, 17 k polystyrene sulfonate with 1.26 mM deuterated dodecyltrimethylammonium bromide (open symbols), and 100 ppm cationically modified hydroxylethylcellulose ("JR-400"; courtesy of Unilever) with 1.40 mM deuterated sodium dodecyl sulfate (closed symbols). The products of scattering length density (SLD) and layer thickness (d) have been fitted in the low q range 0.01–0.03 Å^{-1} —where the product of SLD$\times d$ is insensitive to the layer thickness within physically reasonably boundaries— with respect to the total acquisition time after a given zero time stamp. Such NR data are being co-modelling with complementary ellipsometry data to derive the interfacial composition of polymer/surfactant mixtures in a current ILL studentship project (see sect. 5.4).

4 Sample environments

Dedicated sample environments are essential to allow precise control of the experimental conditions. For soft-matter measurements, a highly collimated neutron beam is generally reflected off a fairly large surface and the sample structure can be very sensitive to both temperature and humidity changes. For air/liquid measurements one may have a sample area on the order of 50–100 cm^2 even avoiding the curved meniscus, but for solid/liquid measurements the footprint usually needs to be more conservative. The range of current sample environments appropriate for NR studies in soft matter has been recently described [20]. In the following paragraphs we describe a range of standard sample environments that have been designed and implemented on the instrument.

4.1 Adsorption troughs

The FIGARO adsorption troughs (fig. 12A) for studying the structure and composition of surface layers self-assembled from solution were designed in house at the ILL, based on similar equipment previously constructed at ISIS [9]. Each liquid trough is 220 mm long and 50 mm wide. The most common material is PTFE as it is chemically inert and relatively easy to clean, although there are also stainless-steel and Delrin troughs. The liquid volumes required for experiments are on the order of 25–50 cm^3 depending on the surface tension of the solution. Six troughs are available on a sample changer, the benefit of which is to measure some samples whilst others are reaching steady state.

Each trough sits in an inner sealed box, complete with sapphire windows before and after the sample. A 250 W silicone rubber mat strip heater (Hawco, Surrey, UK) is fixed to the length of the underside of each inner box to allow measurements above ambient temperature. Additionally, there are troughs configured with water cooling circuits to allow measurements below ambient temperature. All six trough boxes sit in a large outer box also with sapphire windows before and after each sample. Large strip heaters traverse the whole length of the outer box to avoid condensation on the outer windows. An optical sensor (Keyence, Japan, LKG-152) positioned above the assembly is used to regulate the sample height automatically, which is particularly useful for surfaces that are weakly reflecting to neutrons, such as monolayers on air contrast matched water. There is a heated, tilted, rotatable quartz window incorporated in a narrow fixed part of the lid of the outer box above each trough. The windows allow the optical sensor to be used whilst the inner boxes are sealed. Routines have been incorporated into the instrument control software

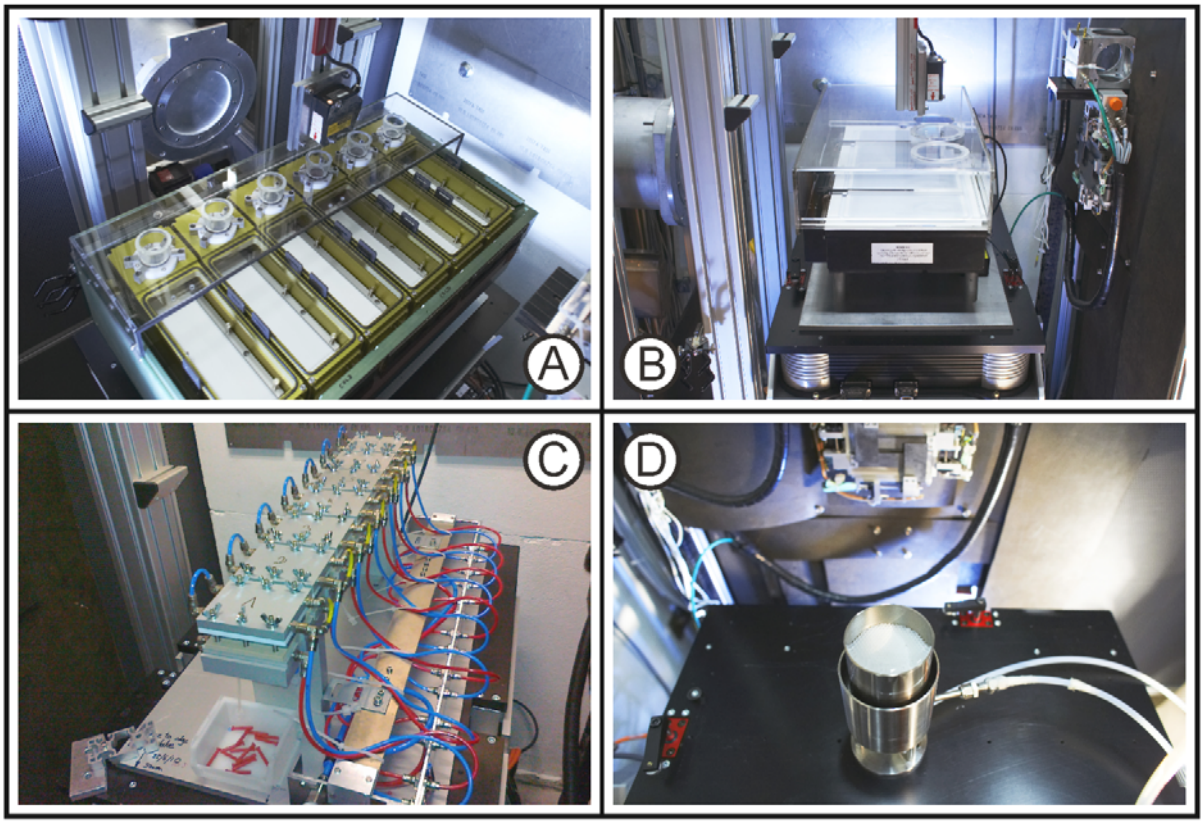

Fig. 12. Photographs of four sample environments taken in the FIGARO sample area: (A) adsorption troughs, (B) Langmuir trough, (C) solid/liquid cells and (D) overflowing cylinder.

NOMAD to align automatically free liquid samples both horizontally and vertically, and to maintain alignment of liquid surfaces.

4.2 Langmuir trough

A Langmuir trough is a container of liquid (usually aqueous media) in which movable barriers regulate the surface pressure of spread films [21]. A Nima BAM-1000 trough (fig. 12B) optimised for high-flux fast measurements is available on the instrument with an area of 100 cm^2 using volumes of around 600 cm^3. A lower-volume Teflon mould insert is available for the use of precious biological samples in volumes less than 150 cm^3. The device is used in the study of insoluble monolayers where the surface pressure, and in cases the phase behaviour of the monolayer, may be controlled precisely. Applications include studies of the interaction with insoluble monolayers of materials either dissolved or injected into the aqueous subphase or present in the gas phase.

Currently there are two available boxes in which to place the Langmuir trough for measurements. The first involves a fixed aluminium part of the lid where the pressure sensor is fixed, and two removable Perspex parts for easy access to spread the sample. A second gas-tight steel chamber with dedicated feed-throughs for the pressure sensor electronics, gas flow and water thermostating is also available for controlled atmosphere studies. Both boxes have a quartz optical window for the height sensor and sapphire or quartz windows for the neutron transmission, all controlled by contact heaters to prevent condensation.

4.3 Solid/liquid cells

Measurements at the solid/liquid interface involve the transmission of a collimated beam of neutrons through a solid crystal (entering by a side face), reflection at the solid-liquid interface, followed by further transmission of the reflected beam out through the solid crystal (exiting by the opposite side face) [22]. The most common experiments use single crystals of silicon that are highly transparent to neutrons, and dimensions may be on the order of 50–100×50×10–15 mm ($l \times w \times h$). Their reflecting surface must be highly polished to have Å-level roughness over the entire illuminated area to avoid loss of the reflectivity signal. Other solid substrates suitable for NR measurements include quartz and sapphire.

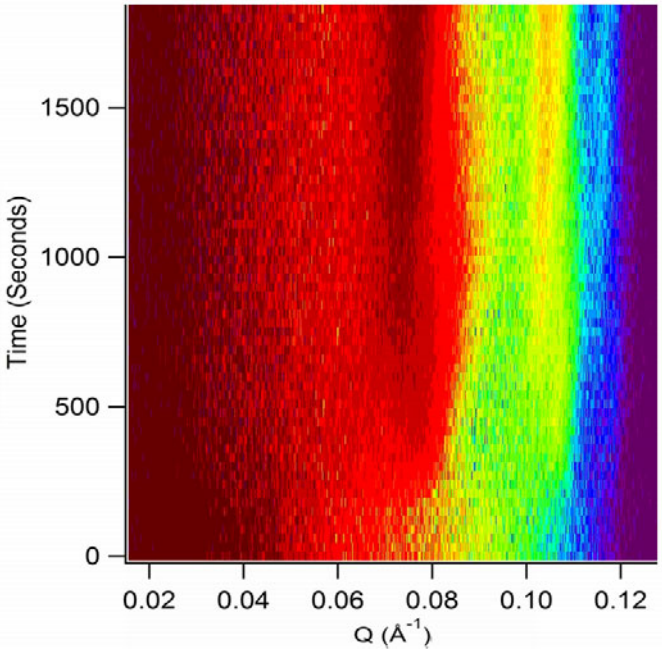

Fig. 13. Time-resolved data set with 30 s time resolution of film formation on a mixed catanionic surfactant solution containing hexadecyltrimethylammonium bromide and sodium dodecyl sulfate with polyacrylamide-co-polymethacrylamidophenylboronic acid-co-poly hexyl methacrylate. Film structure is of the $Im3m$ space group.

The FIGARO sample cells (fig. 12C) are constructed of a single crystal sealed against an o-ring sitting on a rigid PEEK trough with a shallow well (< 0.5 mm) to contain the liquid volume (~ 2 mL inside the cell). The sample cell is held together by clamped hollow blocks of aluminium in which there are drilled circuits for water circulation to thermostat the samples. The sample injection inlet and outlet have thin slits (1 mm) spanning most of the width of the trough allowing efficient laminar flow of the solution. The principal design feature is the low volume of liquid required during solution exchanges, as the cells were developed with biological applications in mind and the availability of deuterated materials is limited. The combination of a high pressure liquid chromatography (HPLC) pump with 4 inlet channels, a mixing chamber and a de-gassing unit (Knauer Smartline 1000) and 6-way valve (Knauer K-6) has been implemented to automate controlled injections into a rack of multiple sample cells.

4.4 Overflowing cylinder

A specialist sample environment that has been configured for the FIGARO beamline is a dynamic flow cell called the overflowing cylinder (fig. 12D), which has been the subject of several non-invasive reflectometry techniques such as NR measurements on the SURF beamline at ISIS [23]. Liquid flows up a vertical cylinder from a gravity-fed reservoir until it spills radially over the top. The expanding liquid surface has been modeled mathematically and several experimental techniques including NR have been applied to pure and mixed surfactant solutions to study the self-assembly of molecules to the expanding surface and characterise adsorption kinetics on short time scales (< 1 s) [24]. As large species in solution have a low diffusion coefficient, the device can be used selectively to distinguish contributions to complex adsorption layers from monomeric and aggregated components and therefore reveal details of the adsorption mechanism. Furthermore, as the surface is constantly regenerated it is possible to distinguish effects of solution and surface aging in multi-component systems with evolving bulk phase behaviour.

5 Early scientific highlights

5.1 Surfactant-templated ordered polymer layers

The formation and mesostructure of polymer/surfactant hydrogel films at the air/water interface [25] was the subject of an experiment by Karen Edler and Jim Holdaway (Bath University, UK). As these films form spontaneously upon mixing of polymer and surfactant solutions and exhibit three dimensionally ordered phases, they are a compelling material for structurally controlled sensors. The control of surfactant-imparted structure in the films using glucose responsive polymers containing phenylboronic acids and alkylated substituents was investigated. The phenylboronic acid moieties reversibly bind saccharides [26] such as glucose whereas the alkyl substituents influence the mesostructure

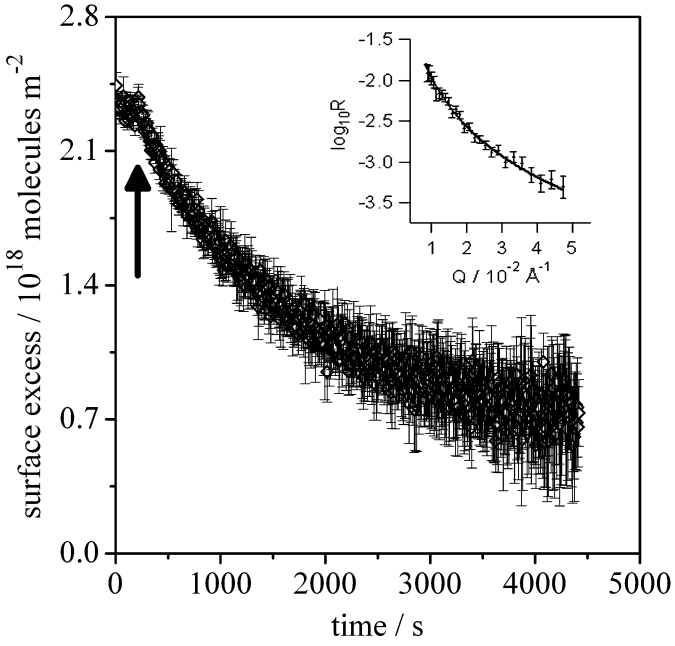

Fig. 14. NR characterisation of the destruction of a deuterated methyl oleate monolayer by nitrous oxides recorded with 6 s time resolution. The arrow marks the start of the active gas flow. The inset shows an example of a reflectivity profile recorded in 1 s used in a fast kinetic study involving ozone.

and provide a soft anchor to hydrophobically modified surfaces [27]. FIGARO was chosen for this work primarily for the horizontal sample orientation, high-flux TOF configuration and two-dimensional detector, thus allowing the study of fast changes in structural anisotropies on the free liquid interfaces. The acquisition of 30 s scans to track structural changes to the $Im3m$ space group represented greater time resolution than had been previously achieved on these films using NR (see fig. 13).

5.2 Gas-phase destruction of methyl oleate monolayers

Modern climate change was the subject of the first scheduled FIGARO experiment, which involved the destruction of organic monolayers on a Langmuir trough by atmospheric gases. Christian Pfrang (University of Reading, UK) and co-workers from Royal Holloway University of London (UK) and Uppsala University (Sweden) looked at the interaction of nitrogen oxides with thin films of organic material in order to mimic processes on cloud droplets in the lower atmosphere. NO_3 is a key night-time oxidant in the atmosphere while the main importance of N_2O_5 lies in its heterogeneous chemistry. Figure 14 shows a kinetic decay of a monolayer of deuterated methyl oleate when exposed to these nitrous oxide gases. The work has shown that the lifetime and fate of organic films on atmospheric aerosols depend strongly on the relative abundance of the competing gas-phase oxidants. The group has achieved data acquisition rates on FIGARO that are two orders of magnitude faster than in their previous experiments [28,29], thus demonstrating the capacity of the instrument to measure fast heterogeneous reactions relevant to atmospheric processes. For example, the inset shows a reflectivity profile of a deuterated methyl oleate monolayer recorded in 1 s, which was used in the study of fast oxidation decays by ozone. Kinetic data obtained from such experiments provide essential input for recently developed modelling approaches for detailed representation of atmospheric aerosols [30].

5.3 Kinetics at high q to determine structural changes in lipid bilayers

The relaxed wavelength resolution (9.8% $d\lambda/\lambda$) on FIGARO was used to measure the effect of phospholipase A_2 enzyme hydrolysis of the structure of a 1-palmitoyl, 2-oleyl-phosphatidylcholine (POPC) lipid bilayer on the minute time scale. Figure 15 shows a series of data sets recorded for 2 min each at an angle of incidence of 3.8°. Hanna Wacklin (ILL, France) showed that as the enzyme hydrolyses the phoshopholipid into a fatty acid and a lyso-phospholipid, a reduction in the surface coverage is seen over time. In contrast to previously published data [31], where the fastest measurement times of 10–15 min were limited to a much smaller q range which allowed only qualitative analysis of the composition, these data also clearly show the evolution in the thickness of the membrane from a bilayer to a much thinner layer (of fatty acid). The increased flux and wide dynamic q range available on FIGARO made these measurements possible. In comparison, previous measurements in a similar q range required 30–45 min measurement times to achieve sufficient statistics [32,33].

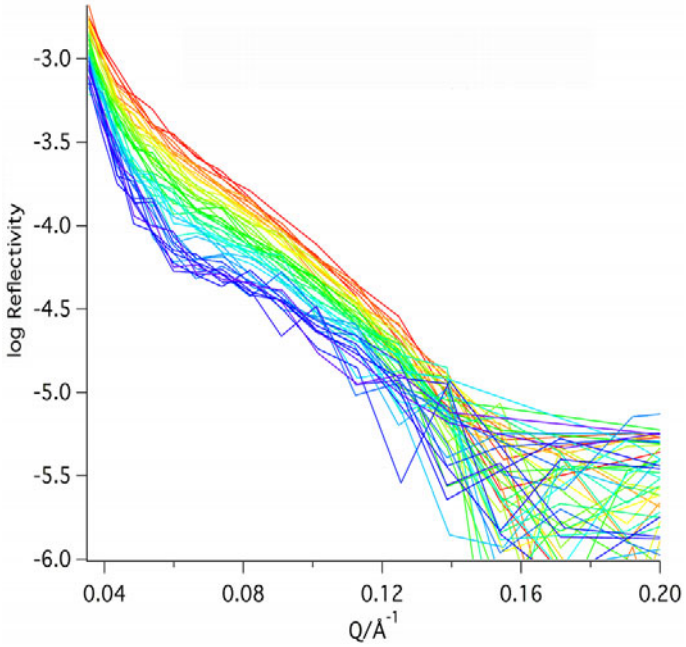

Fig. 15. Hydrolysis of a POPC bilayer by phospholipase A_2 from porcine pancreas (0.01 mg/ml) at the silicon/D_2O interface, recorded for 2 min at 10 min intervals. The changes in reflectivity from the bilayer (red) to a much thinner layer of approximately 50% of the material (blue) indicates that the hydrolysed molecules are solubilised into the subphase.

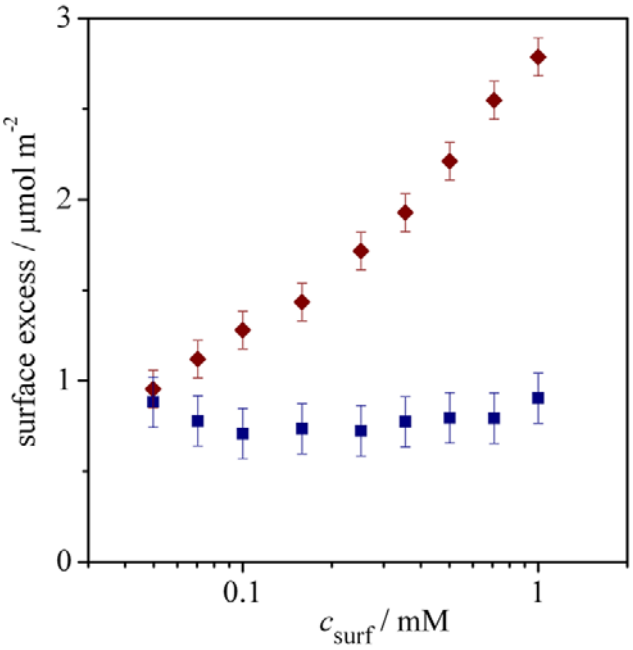

Fig. 16. Interfacial composition of solutions of 17 k, 50 ppm polystyrene sulfonate (blue squares), dodecyl trimethylammonium bromide (red diamonds) in 0.1 M sodium bromide on an overflowing cylinder determined by combined modelling of NR and ellipsometry data.

5.4 Adsorption kinetics at an expanding liquid surface

Bulk solution interactions of oppositely charged polymer/surfactant mixtures result in the formation of nanometer-sized complexes and larger aggregates, all of which can be surface-active but macroscopic aggregates do not diffuse to the sub-surface of the OFC at short time scales. As a result, the device can be used to differentiate between adsorption of various species present in solution and examine the time scale of structural rearrangements at the air/water interface. For example, while Taylor *et al.* observed compact multilayer structures of polystyrene sulfonate (PSS)/dodecyl trimethylammonium bromide (DTAB) mixtures at static free liquid surfaces [34], Anna Angus-Smyth

and Colin Bain (Durham University, UK) showed that the polymer conformation is much more extended on sub-second adsorption time scales. Also, the interfacial composition was derived by co-modelling NR and ellipsometry data: the constancy of the polymer surface excess with respect to the bulk surfactant concentration in fig. 16 is surprising given the non-monotonic trends observed previously for the system poly(diallyldimethylammonium chloride) with sodium dodecyl sulfate [35]. Dissimilarities between these systems can be rationalised in terms of the co-adsorption of bulk complexes and free surfactant to the expanding liquid surface and the different bulk phase behaviour [36].

Concluding remarks

FIGARO is a new world-class neutron reflectometer at the Institut Laue-Langevin in Grenoble, France. Important strengths lie in its high flux, its versatility to tune flux, q range, resolution and instrument geometry for any given experiment, and its expanding range of sophisticated sample environments. The stable reactor source and very fast data acquisition at low q makes the instrument particularly suited to kinetic studies. For example, useful kinetic measurements as short as 1 s have been successfully fitted in user experiments, and the product of scattering length density and thickness for compositional analysis of adsorption layers at the air/water interface can be determined to high precision in less than one minute. Data acquisition over the full q range can be done with just two incident angles in minutes and rarely requires more than one hour. In fact experiments are already taking place on the instrument that are no longer flux limited, but are instead limited by the sheer magnitude of the sample handling. As we look to the future it is clear that advances in sample automation is a key step in turning higher experimental throughput into increased scientific output.

For the scientific case of the instrument we gratefully acknowledge valuable input by R.K. Thomas and A.R. Rennie as well as useful discussions with A. Glidle, A. Zarbakhsh and J. Daillant. For the preliminary design phase we are greatly indebted to advice from R. Gähler and K. Andersen. For the technical realisation we thank all the members of the ILL technical services and the instrument technician S. Wood. We thank J. Webster and S. Holt for helpful discussions during the design of FIGARO's adsorption troughs.

References

1. `http://www.ill.eu/`.
2. R. Cubitt, G. Fragneto, Appl. Phys. A: Mater. Sci. Process **74**, 329 (2002).
3. J.B. Hayter, R.R. Highfield, B.J. Pullman, R.K. Thomas, A.I. McMullen, J. Penfold, J. Chem. Soc. Faraday Trans. I **77**, 1437 (1981).
4. J. Penfold, R.C. Ward, W.G. Williams, J. Phys. E **20**, 1411 (1987).
5. P. Muller-Buschbaum, J.S. Gutmann, R. Cubitt, M. Stamm, Colloid Poly. Sci. **227**, 1193 (1999).
6. Langmuir, Vol. **19**, No. 19 (2003) pp. 7685–8124.
7. Langmuir, Vol. **25**, No. 7 (2009) pp. 3917–4242.
8. J.A. Dura, D.J. Pierce, C.F. Majkrzak, N.C. Maliszewskyj, D.J. McGillivray, M. Lösche, K.V. O'Donovan, M. Mihailescu, U. Perez-Salas, D.L. Worcester, S.H. White, Rev. Sci. Instrum. **77**, 074301 (2006).
9. J. Penfold, R.M. Richardson, A. Zarbakhsh, J.R.P. Webster, D.G. Bucknall, A.R. Rennie, R.A.L. Jones, T. Cosgrove, R.K. Thomas, J.S. Higgins, P.D.I. Fletcher, E. Dickinson, S.J. Roser, I.A. McLure, A.R. Hillman, R.W. Richards, E.J. Staples, A.N. Burgess, E.A. Simister, J.W. White, J. Chem. Soc. Faraday Trans. **93**, 3899 (1997).
10. T.R. Charlton, R.L. Coleman, R. Dalgliesh, C.J. Kinane, C. Neylon, S. Langridge, J. Plomp, N.G. Webb, J.R. Webster, Neutron News **22**, 15 (2011).
11. M. James, A. Nelson, S.A. Holt, T. Saerbeck, W.A. Hamilton, F. Klose, Nucl. Instrum. Methods A **632**, 112 (2011).
12. S.C.M. Teixeira *et al.*, Chem. Phys. **345**, 133 (2008).
13. A.A. van Well, Physica B **959**, 180 (1992).
14. H. Schober, *Neutron Scattering Applications and Techniques*, in *Neutron Imaging and Applications*, edited by I.S. Anderson, R. McGreevy, H.Z. Bilheux (Springer, 2009) Chapt. 3.
15. C. Fradin, A. Braslau, D. Luzet, D. Smilgies, M. Alba, N. Boudet, K. Mecke, J. Daillant, Nature **403**, 871 (2000).
16. T. Seydel, M. Tolan, B.M. Ocko, O.H. Seeck, R. Weber, E. DiMasi, W. Press, Phys. Rev. B **65**, 184207 (2002).
17. N. Kardjilov, A. Hilger, I. Manke, M. Strobl, M. Dawson, J. Banhart, Nucl. Instrum. Methods A **605**, 13 (2009).
18. H. Kiessig, Ann. Phys. (Leipzig) **10**, 715 (1931).
19. A. Nelson, J. Appl. Cryst. **39**, 273 (2006).
20. P. Lindner, R. Schweins, R.A. Campbell, *Sample Environment for Small-Angle Neutron Scattering and Neutron Reflectometry*, in *Neutrons in Soft Matter*, edited by T. Imae, T. Kanaya, M. Furusaka, N. Torikai (Wiley, Hoboken, New Jersey, 2011) Chapt. III-5.
21. G.L. Gaines, *Insoluble Monolayers*, 1st edition (Wiley, 1966).

22. D.C. McDermott, J.R. Lu, E.M. Lee, R.K. Thomas, A.R. Rennie, Langmuir **8**, 1204 (1992).
23. S. Manning-Benson, S.R.W. Parker, C.D. Bain, J. Penfold, Langmuir **14**, 990 (1998).
24. C.D. Bain, Adv. Colloid. Interf. Sci. **144**, 4 (2008).
25. K.J. Edler, M.J. Wasbrough, J.A. Holdaway, B.M.D. O'Driscoll, Langmuir **25**, 4047 (2009).
26. G. Springsteen, B. Wang, Tetrahedron **58**, 5291 (2002).
27. I.G. Sedeva, D. Fornasiero, J. Ralston, D.A. Beattie, Langmuir **25**, 4514 (2009).
28. M.D. King, A.R. Rennie, C. Pfrang, A.V. Hughes, K.C. Thompson, Atmos. Environ. **44**, 1822 (2010).
29. M.D. King, A.R. Rennie, K.C. Thompson, F.N. Fisher, C.C. Dong, R.K. Thomas, C. Pfrang, A.V. Hughes, Phys. Chem. Chem. Phys. **11**, 7699 (2009).
30. C. Pfrang, M. Shiraiwa, U. Pöschl, Atmos. Chem. Phys. **10**, 4537 (2010).
31. H. Vacklin, F. Tiberg, G. Fragneto, R.K. Thomas, Biochemistry **44**, 2811 (2005).
32. H.P. Wacklin, Biochemistry **48**, 5874 (2009).
33. H.P. Wacklin, F. Tiberg, G. Fragneto, R.K. Thomas, BBA-Biomembranes **1768**, 1036 (2007).
34. D.J.F. Taylor, R.K. Thomas, J. Penfold, Langmuir **18**, 4748 (2002).
35. R.A. Campbell, P.A. Ash, C.D. Bain, Langmuir **23**, 3242 (2007).
36. R.A. Campbell, A. Angus-Smyth, M.Y. Arteta, K. Tonigold, T. Nylander, I. Varga, J. Phys. Chem. Lett. **1**, 3021 (2010).